Effect of Carbon-Based Particles on the Mechanical Behavior of Isotactic Poly(propylene)s

Cristhian Garzon,* Manfred Wilhelm, Mahdi Abbasi, Humberto Palza

Different carbon-based fillers such as carbon nanotubes (CNTs), graphite, and thermally reduced graphene oxide (TrGO) are melt mixed with an isotactic poly(propylene) (iPP) and the mechanical properties of the resulting composites in the solid and melt state are analyzed. The Young's modulus of composites is increased around 25% relative to the neat iPP at concentrations above 10 wt% of CNTs or graphite whereas composites with TrGO are increased around 40% at similar concentrations. These results are compared with theoretical models showing that the filler agglomeration and surface area are key parameters. The rheological results of the composites under oscillatory shear conditions at the melt state show that the viscous raw polymer melt experiences a solid-like transition at a threshold concentration that strongly depends on the filler used. This transition appears at 10 wt% for CNTs, 8 wt% for TrGO, and 40 wt% for graphite. The viscosity of iPP/TrGO composites is further increased by adding CNTs particles, although the Young's modulus does not increase.

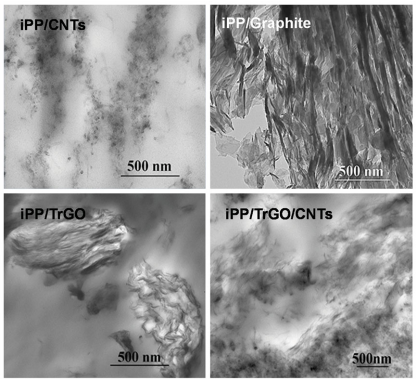

1. Introduction

Polymer nanocomposites have yielded novel advanced functional materials with improved properties such as electrical conductivity, magnetic, mechanical strength, barrier properties, and thermal stability,[1–6] consequently extending their use in many engineering fields,[7] for versatile applications such as environmental remediation, electromagnetic (EM) absorption, energy storage, saving storage, and anticorrosion, among others.[8,9] From the different types of nanoparticles used as filler, carbon-based materials are highlighted, especially carbon nanotubes (CNTs) due to their outstanding properties such as thermal stability (> 700 °C in air), high modulus (≈ 1 TPa), aspect ratio (≈ 1000), and electrical conductivity (≈ 10^6 S m^{-1}).[1] The CNTs are mainly used in the development of composite materials taking advantage of either electrical conductivity by forming a percolated network,[10,11] or improved mechanical properties by filler reinforcement.[1,12–16] For the former application, the addition of a second nanoparticle forming a hybrid nanocomposite to improve the electrical behavior is stressed allowing the reduction of CNTs concentration in the percolated system.[10,17–22] This approach has not been tested toward mechanical behavior. However, CNTs present a major drawback related with its high cost explaining the large interest during the last years in polymer composites based on less expensive carbon nanostructures having also high aspect ratio such as those derived from graphite or even carbon black.

C. Garzon, H. Palza
Departamento de Ingeniería Química y Biotecnología
Facultad de Ciencias Físicas y Matemáticas
Universidad de Chile
Beauchef 861, Casilla 277, Santiago, Chile
E-mail: cgarzon@ing.uchile.cl
M. Wilhelm, M. Abbasi
Institut für Technische Chemie und Polymerchemie
Karlsruhe Institute of Technology (KIT), Engesserstrasse 18
76131 Karlsruhe, Germany

DOI: 10.1002/mame.201500380

Graphite is the most stable carbon form at standard conditions[17] having a current annual global production of around 1.11 million tons and a value around of U$ 1150 ton^{-1} during 2013.[23] Nanoparticles based on modified graphite, such as graphene and its derivatives, have emerged as fillers with the potential to replace expensive CNTs.[24] Graphene has extraordinary properties such as a Young's modulus of 1 TPa, tensile strength of 130 GPa, and electrical conductivity of ≈10^5 S m^{-1}.[25–27] These properties along with its extremely high specific surface area (around 2630 m^2 g^{-1}) and impermeability to gases, show the great potential of either graphene or its derivatives, as fillers for improving the properties of polymers, for instance, electrical, mechanical, and barrier.[26] Graphene derivatives coming from the chemical modifications of graphite are highlighted due to their potential scaled up production. These top-down methods break the sp^2 bonds of graphite by using strong oxidizing agents, for instance, by the Hummers process,[28] forming functional groups such as hydroxyl, epoxide, carboxyl, and carbonyl, within the graphite structure and producing graphite oxide (GO) particles.[28,29] The presence of these functional groups largely reduces the thermal stability and the electrical conductivity of GO,[26,30] although by a reduction process these properties can be mostly regained.[25] In particular, by a thermal shock at high temperatures under inert atmospheres, such as Ar or N_2, GO can be reduced, resulting in thermally reduced graphene oxide (TrGO).[11,29,31] This process removes the functional groups while significantly exfoliates the structure increasing the surface area.[30,32] Both the evaporation of water and the elimination of oxide groups can cause a loss of mass ≈30%, leaving vacancies and structural defects (wrinkles) generally reducing the mechanical and electrical properties of TrGO.[25,30] However, the bulk conductivity of TrGO is between ≈10^3 and 10^4 S m^{-1}, suggesting an effective reduction of GO and restoration of the electronic structure of the material.[25] Based on these properties, TrGO can be considered as a suitable filler for the development of functional polymeric nanocomposites, usually based on polar matrices. This is achieved by using frequently the solution-[26,33–35] or melt-mixing methods[36] or combinations of both.

Polyolefins, such as isotactic poly(propylene) (iPP) and polyethylene (PE), represent more than 50% of the market of commodity thermoplastics, despite this nanocomposites with TrGO have been barely developed. The homogeneous dispersion of carbon-based fillers is not easy to achieve, especially in nonpolar polymer matrices such as polyolefin because carbon-based fillers tend to form aggregates that are thermodynamically stabilized by van der Waals forces and numerous π–π interactions between the fillers. Kim et al.[37] successfully create PE/TrGO nanocomposites (5 wt%) achieving an increase of around 60% in the tensile modulus compared with neat PE by either solution- or melt-mixing techniques. Nanocomposites of iPP/TrGO have also been prepared by melt mixing,[11,29,38,39] although other techniques such as in situ polymerization have been reported.[40,41] These iPP composites with concentrations of about ≈5 wt% of TrGO presented improved electrical conductivity (around 10^{-7} S m^{-1}), an increase around 500 MPa in the Young's modulus of the composite compared to the matrix,[29,38,39] and further showing higher Young's modulus than the other composites, for instance, iPP/CNTs.[29]

Polymer composites with carbon based materials have also been studied focusing on the melt rheology due to its importance for both the understanding of the processing operations and the analysis of the microstructure of the material.[30] Moreover, rheology can detect the presence of complex morphologies, such as a percolated structure associated to the formation of a 3D network of nanoparticles along the nanocomposite,[42,43] This network changes the behavior of the melt matrix at low shear rates and low frequencies from a liquid-like Newtonian fluid to a solid-like Hooke fluid. The dependence of viscoelastic parameters on the concentration of carbon-based filler has been widely studied in the literature for polymer composites with CNTs,[44–58] but little has been addressed in composites with other fillers such as graphite,[59–61] and/or TrGO.[36,45,60,62,63] Isotactic poly(propylene) nanocomposites with CNTs have a rheological percolation at concentrations between 0.3 and ≈ 3 wt%,[45,49,51,56–58] while iPP/TrGO composites require concentration above 5 wt% to achieve rheological percolation,[45] showing that the size and aspect ratio of the carbon-based filler affect the melt rheology of the composite.

Our group previously published the strong dependence of the kind of carbon-based filler on the electrical behavior of iPP composites with multiwall CNTs displaying the smallest electrical percolation threshold as compared with TrGO and graphite.[11] These results motivated us to further extend the analysis to other relevant properties especially mechanical behavior in both solid and melt state being the main goal of this contribution.

2. Experimental Section

2.1. Materials

A commercial grade isotactic poly(propylene) from Petroquim S.A. (Chile) (PH0130) with a melt flow rate of 1.7 g 10 min^{-1} at 230 °C and 2.16 kg, M_w = 360 kg mol^{-1}, M_n = 70 kg mol^{-1}, PDI = 5.1, and melting point of 160 °C was used as matrix. Graphite (graphite fine powder extra pure) with a particle size < 50 μm, sulfuric acid (98.08 wt%, H_2SO_4), potassium permanganate (99 wt%, $KMnO_4$), hydrochloric acid (32 wt%, HCl), and sodium nitrate (99.5 wt%, $NaNO_3$) were obtained from Merck (Germany) and used as

received. Hydrogen peroxide (5 vol%, H_2O_2) was purchased from Kadus S.A. The multiwalled carbon nanotubes (MWCNT) were obtained from Bayer Material Science AG (Germany) (Baytubes C150P). Based on the datasheet information provided by Bayer, they are characterized by a purity higher than 95 wt%, number of walls between 2 and 15, an outer mean diameter of 13–16 nm, an inner mean diameter of 4 nm, and length between 1 and 10 μm. Irganox 1010 was obtained from Ciba-Geigy and used as antioxidant agent during the composite preparation.

2.2. Preparation of TrGO

The TrGO was prepared in a two-step oxidation/thermal reduction process using graphite as raw material. The graphite oxidation process of Hummers and Offeman was employed,[28] with $KMnO_4$ and $NaNO_3$ as oxidants in concentrated sulfuric acid, as described in ref.[11]. In a second step, the dry GO was thermally reduced to afford TrGO in a nitrogen atmosphere by rapidly heating GO up to ≈ 600 °C during 40 s using a quartz reactor heated in a vertical tube furnace. The thermal shock is the prime requirement to achieve exfoliation of graphene sheets.

2.3. Melt Compounding

The composites were prepared using a Brabender Plasticorder (Brabender, Germany) internal mixer at 190 °C and a speed of 110 rpm. ≈ 30 g per mixing was produced, containing iPP, filler (CNTs, TrGO, or graphite), and ≈ 5 mg of Irganox 1010 as antioxidant. Filler content ranges from 0 to 25 wt% for TrGO or CNTs, and from 0 to 45 wt% for graphite. First, iPP was mixed with antioxidant and subsequently half amount of the polymer (≈ 13 g) was added to the mixer operated at 110 rpm. After 2 min the iPP was melted and the filler was added for 3 min. Finally, the rest of the polymer pellets were added and the speed of the mixer was held at 110 rpm for 10 min. Therefore, the total mixing time was around 15 min. For the hybrid materials, first the polymer was added to the mixer followed by the proper amount of TrGO (5 wt%) as above explained and afterward, the desired amount of the CNTs (from 0 to 5 wt%) was added. In this case, the same process conditions of the binary mixtures were used and the total mixing time was also around 15 min.

2.4. Characterizations

The morphology and microstructure of the nanocomposites were determined by transmission electron microscopy (TEM) in a Tecnai F20 FEG-S/TEM operated at 120 kV, equipped with an energy dispersive X-ray analysis system (EDS). Ultrathin sections of about 70 nm were obtained by cutting the samples with a Sorvall Porter-Blum MT2-B ultra-microtome equipped with a Diatome diamond knife. Young's modulus and elongation at break were tested on a HP model D-500 dynamometer according to ASTM D638-10 at ≈ 25 °C. For these tests, samples bone type with overall length of 120 mm, distance between grips of 80 mm, width of narrow section of 11.5 mm, and thickness of 1 mm were tested at a strain rate of 50 mm min^{-1} at room temperature. The results presented here are the average values out of five measurements (typical deviation ≈ 5% in modulus). Differential scanning calorimetry (DSC) curves were performed using a TA Instruments differential scanning calorimeter, model DSC Q20, operating at a heating rate of 10 °C min^{-1} and a temperature range from −40 to 200 °C. Melting temperature, T_m, was determined in the second scan and the degree of crystallinity was calculated from enthalpy of fusion data obtained from the DSC curves (209 J g was used for 100% crystalline material).[40,45,64] Rheological measurements were run on an ARES-G2, TA-Instruments rheometer with 25 mm parallel plate geometry conducting an isothermal frequency sweep at 190 °C with ω = 0.01–100 rad s^{-1}. All measurements were conducted in the linear (mechanical response) regime, with deformation amplitude γ_0 = 3%, and under nitrogen atmosphere to avoid oxidative degradation.

3. Results and Discussion

3.1. Morphology of Poly(propylene) Composites with Carbon-Based Particles

Figure 1 shows TEM images of the composites showing the effect of different carbon-based fillers on their morphologies. In particular, Figure 1a shows that CNTs were mainly presented as aggregates, or bundles, with sizes around 500–600 nm into the polymer matrix although small ropes formed by a few individual CNTs were also observed.[65] The CNTs aggregates were continuously interconnected through the polymer by means of these lonely CNTs allowing the electrical conduction in these samples as reported previously.[11,65] Figure 1b shows a representative image from composites based on micrometric graphite particles having a dense layered structure. A much less dense structure was observed in composites based on TrGO

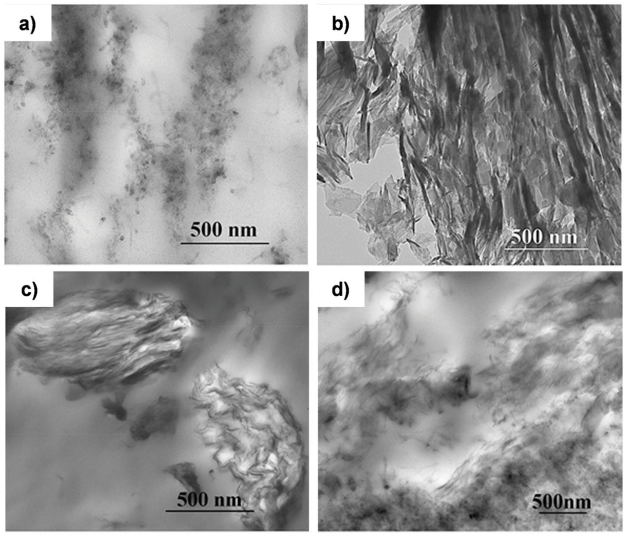

Figure 1. Representative TEM images of the composites studied: a) iPP with ≈ 10 wt% of CNTs filler; b) iPP with ≈ 10 wt% of graphite filler; c) iPP with ≈ 10 wt% of TrGO filler; and d) iPP composites with 5 wt% of TrGO and 2 wt% of CNTs fillers.

as displayed in Figure 1c, where the graphene nanoplatelets were intercalated and wrinkled due to the presence of the polymer matrix. Moreover, the polymer was able to disrupt the agglomerations and particles of less than 1 μm were observed. Figure 1d shows the improvement in the dispersion of the wrinkled structure of TrGO by the simultaneously addition of CNTs.[11,29,30,65]

3.2. Mechanical Tensile Properties

Figure 2 shows the variation of Young's modulus and elongation at break of iPP and its composites with the different fillers, leading to the conclusion that the mechanical behavior of the composites depended on both the concentration and the type of carbon-based filler. The Young's modulus (Figure 2a) of iPP/CNTs and iPP/graphite composites increased almost linearly with filler concentration, regardless of the filler. The iPP composites with TrGO however displayed Young's modulus (at room temperature) ≈ 200 MPa higher than the other composites at the same concentrations resulting in about 15% increase. The highest increase exhibited by composites with TrGO can be explained by its high aspect ratio and strong interfacial bonding due to its rough and wrinkled texture of TrGO caused by oxygen functionalization and the defects during thermal exfoliation of graphite oxide increasing the mechanical attachment with the matrix as has been reported in other publications,[30,34,66,67] and also observed here, see in Figure 1c. Regarding the hybrid composites with TrGO and CNTs, despite they exhibit better filler dispersion within the matrix (Figure 1d) a significant improvement in modulus or elongation at break (Figure 2b) was not observed as compared with composite with 5 wt% of TrGO, even at concentrations of 5 wt% of CNTs.

Table 1 displays the main thermal properties. The crystallinity degree of the samples was calculated by

$$X_c = \frac{\Delta H_m}{(1-w_t)\Delta H_o} \quad (1)$$

where ΔH_m is the experimental melting enthalpy of the sample, ΔH_0 is the theoretical melting enthalpy of the 100% crystalline iPP with a value of 209 J g,[40,45,64] and w_t is the weight fraction of filler in the composite. Although the increase in the crystallization temperature, T_c, of poly(propylene) indicates that the carbon-based fillers are acting as nucleating agents, favoring the crystallization process,[41] in general, both the amount of crystalline phase, X_c, and melting temperature, T_m, were not greatly affected neither by the presence of these fillers nor by its concentration. For instance, a variation of less than 5% in both X_c and T_m, was found between iPP ($T_m \approx 161.3$ °C and $X_c \approx 53\%$) and iPP + 10 wt% of TrGO ($T_m \approx 163.1$ °C and $X_c \approx 53\%$), similarly as reported by Guo and co-workers.[44,45] Therefore, changes in Young's modulus are just explained by the presence of the carbon-based particles rather than by changes in crystallinity.

Figure 2b shows the decrease in elongation at break of the different composites as the concentration of carbon-based fillers is increased, especially when CNTs, TrGO, or both together (hybrid composites) were used. In particular, for incorporations higher than 2 wt% of filler, the nanocomposites were brittle having an ≈ 50% drop in the elongation at break as compared with iPP.

The composite mechanical properties depend on the concentration and distribution of the reinforcing phase, within the matrix, the polymer–filler bonding interface, and the filler aspect ratio, among other variables.[25] The increased Young's modulus in iPP composites with carbon-based fillers was similar to that reported by Steurer et al.[29,68] and Milani et al.[41] but differed from the results of Fang and co-workers[39] and Torkelson and co-workers[61,69] reporting a maximum value followed by a decrease at filler concentrations above 2 and 10 wt%, respectively. On the other hand, the decreased elongation at break of our iPP composites is related to the possibility of crack formation as previously reported in the literature.[29,38,39] The mechanical behavior of iPP composites prepared in the present study, and values reported by

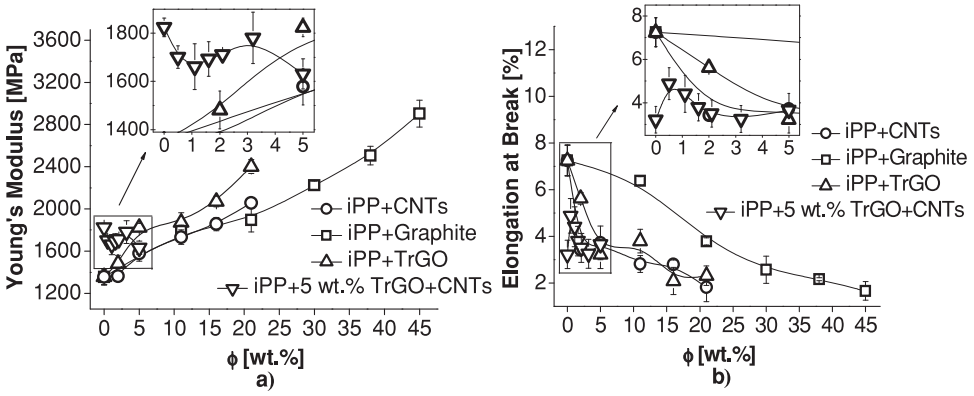

Figure 2. Variation in a) Young's modulus, and b) elongation at break with the increase in the concentration of carbon-based filler.

Table 1. Melting and crystallization characteristics of neat iPP and iPP composites with different carbon-based fillers.

Material	ΔH_m [J g^{-1}]	T_m [°C]	T_c [°C]	X_c [%]
iPP	110.8	161.3	116.3	53
iPP + 5 wt% CNTs	104.4	163.6	122.1	50
iPP + 10 wt% CNTs	107.0	163.9	123.7	51
iPP + 15 wt% CNTs	116.4	163.5	129.8	56
iPP + 20 wt% CNTs	113.8	163.5	130.5	55
iPP + 10 wt% graphite	106.8	164.3	124.4	51
iPP + 20 wt% graphite	104.6	163.9	126.4	50
iPP + 30 wt% Graphite	113.0	163.9	127.4	54
iPP + 40 wt% graphite	113.7	164.4	129.3	52
iPP + 45 wt% graphite	107.8	165.2	131.5	50
iPP + 5 wt% TrGO	118.6	160.7	122.8	56
iPP + 10 wt% TrGO	111.1	163.1	124.8	53
iPP + 15 wt% TrGO	97.9	162.2	124.6	47
iPP + 20 wt% TrGO	102.5	163.5	127.0	49

other investigators at similar concentrations (although the way to disperse is different), are summarized in Table 2.

The increase in stiffness in composites can be understood by the stress transfer between the continuous phase and the dispersed phase[70–72] and can be calculated using the equation proposed by Halpin and Tsai assuming perfect interaction (or adhesion) between the polymer matrix and the particle.[73] This model can be used for composites with continuous (fiber-reinforced composites) and discontinuous (particulate composites) fillers as well as for a variety of unidirectional or randomly distributed forms.[39,74] The Young's modulus of the composites with particles randomly distributed (E_{random}) and aligned parallel to the direction of stress (E_{parall}) are given by[39,66]

$$E_{random} = E_m\left[\frac{3}{8}\frac{1+\xi\eta_l v_f}{1-\eta_l v_f}+\frac{5}{8}\frac{1+2\eta_t v_f}{1-\eta_t v_f}\right] \quad (2)$$

$$E_{parall} = E_m\left[\frac{1+\xi\eta_l v_f}{1-\eta_l v_f}\right] \quad (3)$$

$$\eta_l = \frac{(E_f/E_m)-1}{(E_f/E_m)+\xi} \quad (4)$$

$$\eta_t = \frac{(E_f/E_m)-1}{(E_f/E_m)+2} \quad (5)$$

$$\xi = 2\left(\frac{(w+l)/2}{t}\right) \quad (6)$$

$$\xi = 2\alpha \quad (7)$$

Table 2. Mechanical behavior of iPP composites with different carbon-based fillers.

Filler	Increment Young's modulus [%]	Decrease Elongation at break [%]	References
5 wt% CNTs	16	49	This work
5 wt% CNTs	20	96	Steurer et al.[29,68]
5 wt% CNTs	7	73	Dittrich et al.[38]
10 wt% CNTs	28	61	This work
10 wt% CNTs	35	98	Steurer et al.[29,68]
2 wt% graphite	101	31	Torkelson and co-workers[61,69]
2 wt% graphite	63	31	Fang and co-workers[39]
5 wt% graphite	21	100	Fang and co-workers[39]
10 wt% graphite	32	12	This work
10 wt% graphite	51	98	Torkelson and co-workers[61,69]
45 wt% graphite	114	77	This work
5 wt% TrGO	35	56	This work
5 wt% TrGO	17	12	Milani et al.[41]
5 wt% TrGO	43	98	Steurer et al.[29,68]
5 wt% TrGO	34	87	Dittrich et al.[38]
10 wt% TrGO	38	48	This work
20 wt% TrGO	77	68	This work
20 wt% TrGO	50	30	Milani et al.[41]

where E_f and E_m represent the Young's modulus of the filler (see Table 3) and matrix (≈ 1.36 GPa), respectively; v_f is the volume fraction of particles measured assuming a density of TrGO, and graphite of ≈ 2.2 g cm^{-3},[30] and ≈ 2 g cm^{-3} for CNTs;[65] η_l and η_t are parameters of longitudinal and transverse reinforcement, respectively, which depend on the E_f and E_m; and ξ is a measure of reinforcement geometry depending on the loading conditions and the aspect ratio of the reinforcement. This parameter (ξ) for TrGO can be expressed as in Equation (6) assuming rectangular filament fillers where l, w, and t represent the length (≈ 500 nm), width (≈ 500 nm), and average thickness (≈ 1.75 nm) of the particle, respectively.[26,31,39,66] In the case of graphite and CNTs, this parameter depends on the aspect ratio, $\alpha = l/r$, where r represents the radius of the particles (Equation (7)).[74] For CNTs, the values of l and the average diameter ($2r$) are ≈ 1 μm and ≈ 16 nm, respectively (datasheet information). For graphite particles, the aspect ratio is ≈ 1, measured roughly by SEM,[11] assuming that they are spherical particles. According to the above mentioned equations two types of Young's modulus (E_{random} and E_{parall}) can be calculated depending on both the 2D and 3D orientation, and shape of the particle.[39] The Young's modulus (E_f) and parameter (ξ) of different materials used in the present study are summarized in Table 3.

Figure 3 shows the variation of Young's modulus of the composites with particles randomly distributed (E_{random}) and aligned parallel to the direction of stress (E_{parall}). Figure 3a shows that in composites with CNTs, the experimental module does not match the theoretical simulation, independent of the particle alignment (2D aligned CNTs or 3D random CNTs). This is due to the presence of clusters of CNTs with $\alpha \approx 2.8$ as measured roughly by TEM in Figure 1a causing a different behavior as compared with the theoretical simulation assuming individual CNTs with $\alpha \approx 125$. Moreover, these clusters have lower modulus than individual CNTs. According to Karevan et al.,[75] the modulus of the agglomerate is calculated based on rule of mixtures considering the cluster as a composite consisting of CNTs and voids, where the concentration of CNTs is ≈ 65 vol%, reducing the modulus from ≈1 TPa to ≈ 650 GPa. As shown in Figure 3a, by performing these adjustments to the Halpin–Tsai model (Halpin–Tsai 3D random CNTs clusters) an excellent numerical adjustment with the experimental results was obtained.

Figure 3b shows that the experimental and the theoretical predictions from iPP/graphite composites were very similar assuming spherical particles with the distribution of particle sizes and the high degree of anisotropy of graphite explaining the slight differences.[11] Regarding composites with TrGO, Figure 3c shows that by increasing the amount of filler, the Young's modulus does not approach the theoretical values, also attributed to the presence of agglomerates.[11] These agglomerates are confirmed in Figure 1c, decreasing the particle aspect ratio from ≈ 286 to ≈ 2.1 and therefore preventing a larger increase in modulus.[30] The broad distribution of TrGO sizes can also explain changes in modulus as reported by Song et al.[39]

To improve our predictions, we used a modified model developed for polymer/clay nanocomposites taking their complex anisotropic layered morphology into account.[76] In this model, the Young's modulus (E_f) of the filler (layered structure) can be estimated by

$$E_f = \frac{N}{t} \cdot E_s \cdot d_s \tag{8}$$

where N is the number of nanoplatelets per stack (agglomerate) supposed equal for all samples for simplicity with a value of ≈ 120 units approximated by TEM; t is the particle agglomerate thickness (400–500 nm); E_s is the TrGO stiffness (70 GPa); and d_s is the thickness of individual TrGO nanoplatelet (≈ 1.75 nm) by assuming 6–7 layers of graphene.[31] By means of the above mentioned parameters for layered particles poorly dispersed in the polymer matrix, the Halpin–Tsai fitted (3D random layered structure) model predicts elastic modulus very similar to the experimental values, as shown in Figure 3c.

Although standard Halpin–Tsai model (Equations (2) and (3) predicts that the CNTs are the best filler, reaching values of Young's modulus higher than those obtained for graphite or TrGO fillers, the experimental results obtained in this study showed that the best mechanical performance was achieved when TrGO is used as filler. Even the Halpin–Tsai model fitted with the real both aspect ratio and Young's modulus of the agglomerates (Equation (8), predicting closer experimental values are not able to show the superior behavior observed in iPP composites with TrGO. The latter despite the lower values of TrGO agglomerates (≈ 30 GPa) as compared

Table 3. Young's modulus (E_f) and parameter (ξ) of different carbon-based fillers used in the Halpin–Tsai model.

Filler	Young's Modulus (E_f) [GPa]	Parameter (ξ)	References
CNTs	1000	250	Datasheet information
Graphite	15	2	[11,86]
TrGO	70	572	[26,30,31,60]

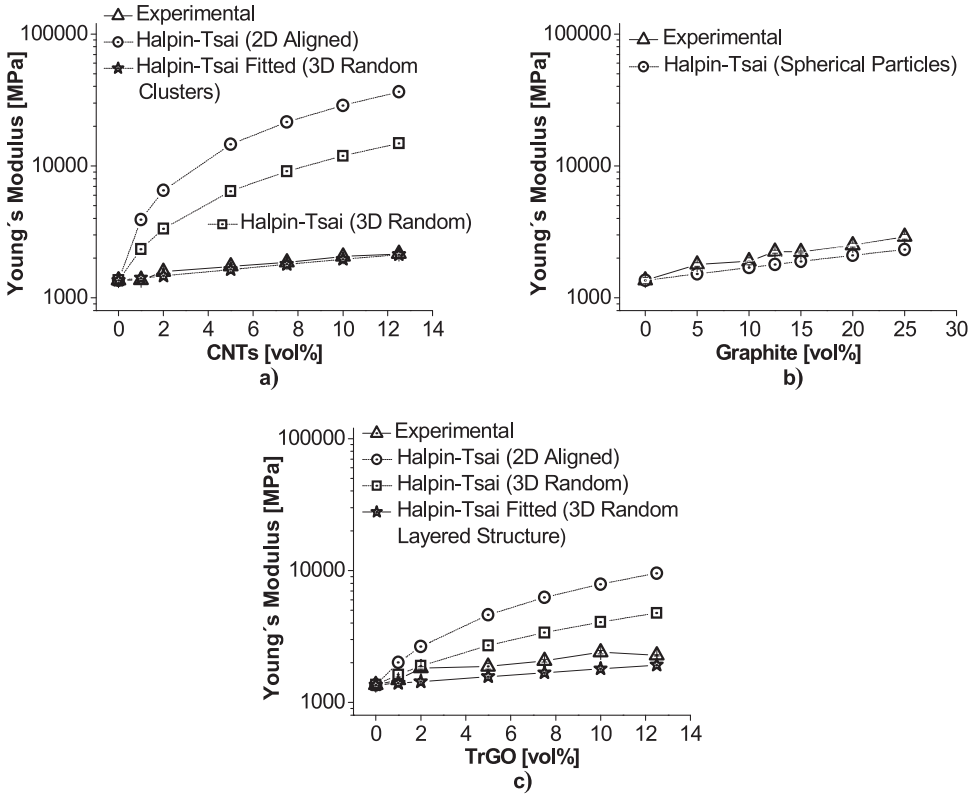

Figure 3. Experimental Young's modulus iPP composites, and calculated results obtained from the Halpin–Tsai model under the assumption that the fillers are randomly dispersed as a 3D network, and aligned in parallel (2D) within composites with a) CNTs, b) graphite, and c) TrGO.

with CNTs agglomerates (≈650 GPa). Therefore, other parameters not contemplated in these models should be responsible for the mechanical improvement of TrGO such as its wrinkled structure and polymer–particle interaction.[30,34,66,67]

3.3. Rheological Behavior of iPP Nanocomposites in the Melt

The viscoelastic behavior of the polymer melt with nanoparticles (storage modulus G' and loss modulus G'') at low frequencies reveals information about the interactions between particles, for instance, the formation of a rigid network of the nanoparticles.[46,62] At high frequencies these tests reflect the motions and mechanical resistance of short polymer segments being less affected by the presence of nanoparticles.[62] Figure 4 shows the dependence of G' on the angular frequency (ω) for the iPP composites with the different carbon-based fillers showing that the neat iPP relaxed at low frequencies with a terminal behavior scaling as $G' \approx \omega^2$.[62] From this figure the strong effect of the carbon-based fillers on the viscoelastic behavior of the poly(propylene) is evident. The pronounced effect is increasing G' by several orders of magnitude as reported for other iPP nanocomposites with CNTs,[7,44,45,51,55–58] graphite,[61] and TrGO.[45,62]

Figure 4a shows a plateau in G' in composites with 10 wt% of CNTs at low frequencies, attributed to the formation of a percolated network within the nanocomposite limiting the polymer relaxations as above discussed.[45,49,51,56,57] Figure 4b shows the rheological characteristics displayed by iPP/graphite composites showing that higher concentrations of filler (> 40 wt%) are needed to modify the viscoelastic behavior as compared with CNTs. A different behavior is observed in iPP/TrGO composites (Figure 4c), as lower G' values than neat iPP in the whole frequency range studied are observed at low concentrations (2 and 5 wt%). Similar results were reported by Guo and co-workers[44,45] who attribute this decrease to the iPP/TrGO interlayer slipperiness due to the low surface friction of graphite. However, as the TrGO concentration increases (≈ 10 wt%), there is an increase of more than two orders of magnitude of G' along with the presence of a plateau. Figure 4d shows that G' of the hybrid composites increased significantly from low concentrations of CNTs, counteracting the interlayer slipperiness of TrGO at low concentrations.

Since G' is more sensitive to the formation of a rigid network by polymer–particle interactions at low frequencies, G' values at 0.01 rad s^{-1} ($G'_{0.01}$) of the different samples were selected and plotted as a function of the volume fraction of filler (ϕ) in Figure 5. Figure 5a shows that $G'_{0.01}$

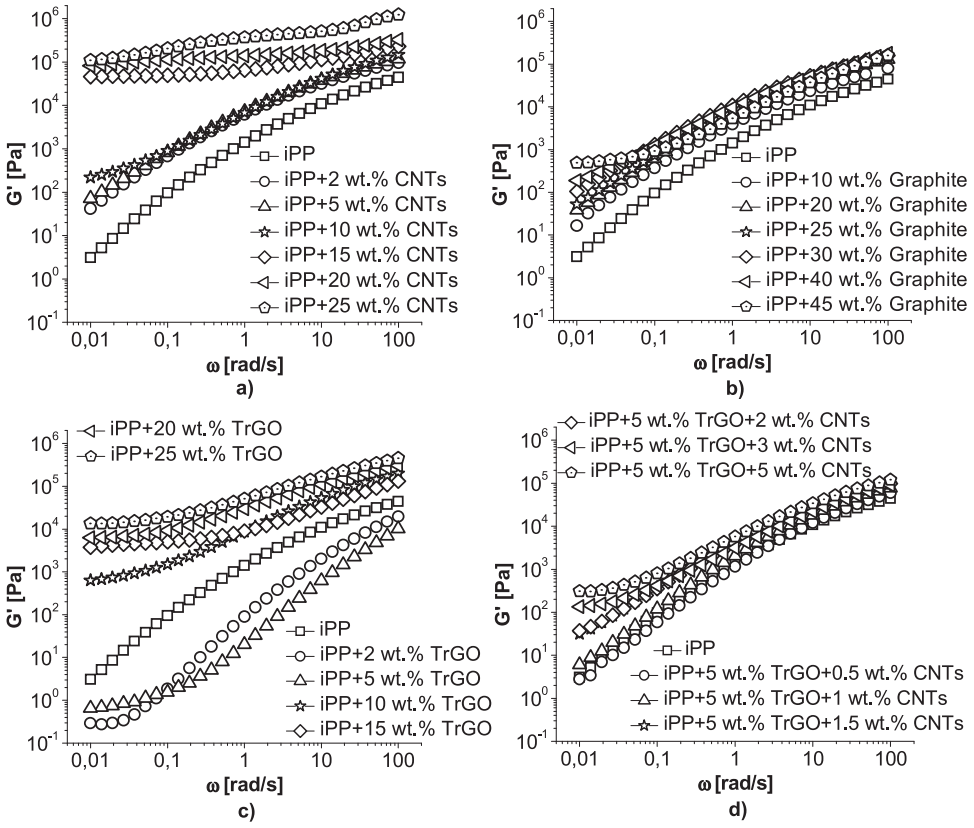

Figure 4. Frequency sweep for the storage modulus (G') of iPP composites as a function of filler concentration by using: a) CNTs, b) graphite, c) TrGO, and d) 5 wt% of TrGO/CNTs at 190 °C and strain $\gamma_0 = 0.03$.

increased dramatically after a critical concentration of filler, since the viscoelastic response of polymer composites changes from viscous to a more elastic melt, showing a nonterminal rheological response at low frequencies.[62] This critical concentration of filler represents the rheological percolation threshold (ϕ_p). Above the threshold, the plateau modulus G' is expected to increase with filler content following a simple power law[36,59,77]

$$G'_{0.01}(\phi) = k(\phi - \phi_p)^v \quad (9)$$

where ϕ is the volume fraction of filler and v is a power law exponent. The value of ϕ_p can be obtained from the linear regression through the data in the power-law region, assuming ($\phi > \phi_p$) as displayed in Equation (9). An expected power law relationship between $G'_{0.01}$ and ($\phi - \phi_p$) at the onset of the rheological percolation is depicted in Figure 5b. The percolation threshold values of iPP composites were ≈ 10 wt% of CNTs, > 40 wt% of graphite, ≈ 8 wt% of TrGO, and 5 wt% of TrGO with > 2 wt% of CNTs. These values clearly indicate that higher aspect ratio particles (i.e., CNTs or TrGO), along with better dispersion (hybrid composites), lead to a lower percolation values (ϕ_p). The fitted v values are in a small range from 0.84 to 1.45 in our study, which are within the range of values (0.7–7) reported for polymer composites with carbon-based fillers.[49,78,79] The discrepancy of v values could be attributed to the selected temperature and frequency used for the G' percolation analyses[48,49,59,78,80,81] or the intrinsic difference in the polymer/carbon-based filler pair.[78]

Tendencies found in Figure 4 could also be associated with changes in the polymer molecular weight during the melt mixing process by degradations reactions. Therefore, the van Gurp–Palmen plot defined as the dependence between the phase angle (δ) and the absolute value of the complex modulus $|G^*|$ measuring the materials overall resistance to deformation, is employed. This plot allowed to show that the presence of carbon-based fillers modifies the rheological behavior of iPP independent of changes in the polymer molar weight.[82] A liquid-like behavior of a melt is indicated by $\lim_{G^*\to 0}\delta = 90^\circ$. For a solid-like behavior δ drops toward zero.[36,46,47,81,82] This is based on the fact that the value of δ is 90° toward $\delta = 0°$ in the low $|G^*|$ region for a polymer melt, provided that the polymer chains are completely relaxed.[78] The deviation of δ from 90° in the low $|G^*|$ region indicates the elastic response of polymer chains by forming a network structure (or percolated network) in the melt sample. For the neat iPP melt used here, the values of δ in the low $|G^*|$ region was ≈88°. This indicates the dominant viscous state. As Figure 6 displays, the

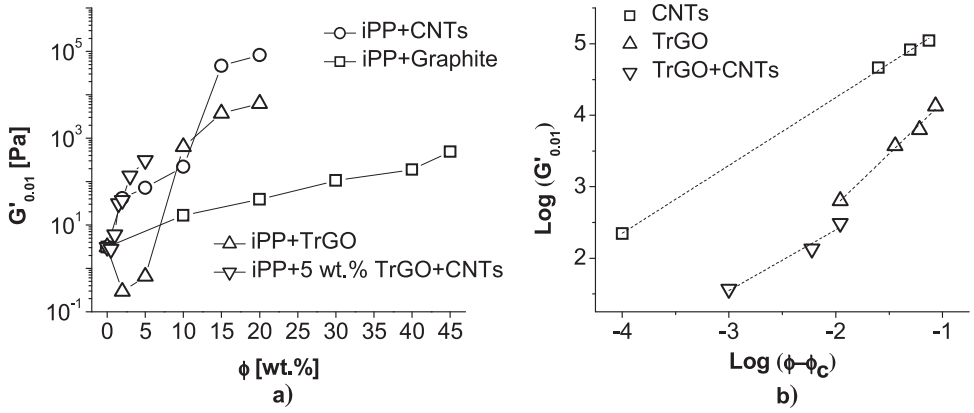

Figure 5. a) Storage modulus (G') at an angular frequency of 0.01 rad s^{-1} for the iPP composites as a function of filler concentration. b) A log-log plot of G' versus reduced mass fraction.

van Gurp–Palmen plots for our composites with low concentrations of filler showed a continuous decrease of δ with $|G^*|$, independent on the kind of carbon particle. At higher concentrations of filler the appearance of a δ maximum is observed associated to the formation of a pseudo-solid-like filler or percolated network.[49]

Similar to the observed in Figures 4 and 5, the transition from liquid- to solid-like behavior in the Van Gurp–Palmen plots (Figure 6) strongly depended on the carbon-based particle. For iPP composites with CNTs (Figure 6a) the viscous-to-elastic melt transitions occurred between 5 and 10 wt% CNTs concentration. Otherwise, iPP composites

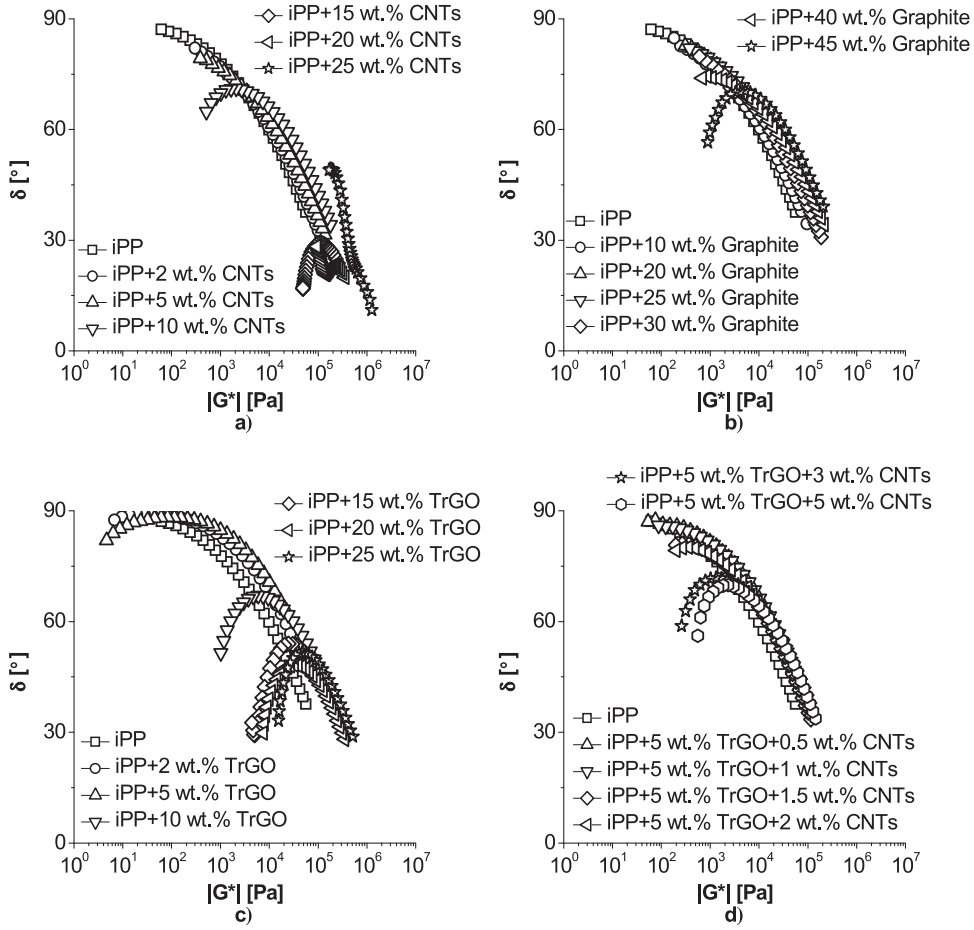

Figure 6. Van Gurp–Palmen plots for the iPP composites with different carbon-based fillers measured at 190 °C.

with graphite filler (Figure 6b) with higher concentrations (≥40 wt%) were required to show a viscous-to-elastic melt transition. For TrGO based composites, Figure 6c shows that to achieve a viscous-to-elastic melt transition, a lower concentration of TrGO (in comparison to CNTs) was needed. Noteworthy, samples with low amount (2 and 5 wt%) of TrGO filler show a deviation of δ from 90° (Figure 6c), confirming that the decrease in relative viscosity is due to the presence of the filler and it is not related to the decrease in the molar weight due to degradation of the polymer chains. Hybrid composites (Figure 6d) display a liquid-to-solid transition is achieved in about 3 wt% of CNTs, decreasing the CNTs concentration necessary to form a percolated network within the material.

Another method[36,49,81] to estimate the rheological percolation threshold is depicted in Figure 7, showing a decrease in the loss tangent (tan δ) with increasing filler concentration at different frequencies. The tan δ of a rheometrical measurement rises by decreasing the angular frequencies ω for liquids, and decreases toward zero for solids.[36] It therefore becomes independent of frequency in the percolation threshold, making lines connecting points measured at the same angular frequency cross. While this is true for homogeneous systems[83] and some heterogeneous composite systems,[49,58] our melt mixed samples showed a frequency-dependent values above the transition similar to that reported by Ratzsch et al.[36]

We chose to use the crossover of the 0.01 and 0.1 rad s^{-1} isolines, since it is the lower range of frequencies where the percolated zone was more easily observable experimentally.

The resulting rheological percolation thresholds ϕ_p (Figure 7) which can be read from the abscissa of the convergence point, are ≈ 8 wt% of CNTs, ≈ 40 wt% of graphite, ≈ 6 wt% of TrGO, and 5 wt% of TrGO with ≈ 2 wt% of CNTs. Samples with low amount (2 and 5 wt%) of TrGO (Figure 7c) were not taken into account because they presented lower G' and G'' than neat iPP, generating miscalculations by this method. These ϕ_p values of composites were very similar to those obtained by adjusting the power-law at low frequency ($\omega = 0.01$ rad s^{-1}) when $\phi > \phi_p$.

The rheological percolation thresholds at concentrations ≈ 10 and ≈ 8 wt% for iPP/CNTs and iPP/TrGO composites, respectively, determined by linear regression of Equation (9) were higher than the electrical percolation values (4 wt% of CNTs and 6 wt% of TrGO) reported previously for these iPP composite materials.[11] The differences among this electrical (DC) and rheological (at $\omega = 0.01$ rad s^{-1}) percolation values can be originated from the different mechanisms for the carbon-based

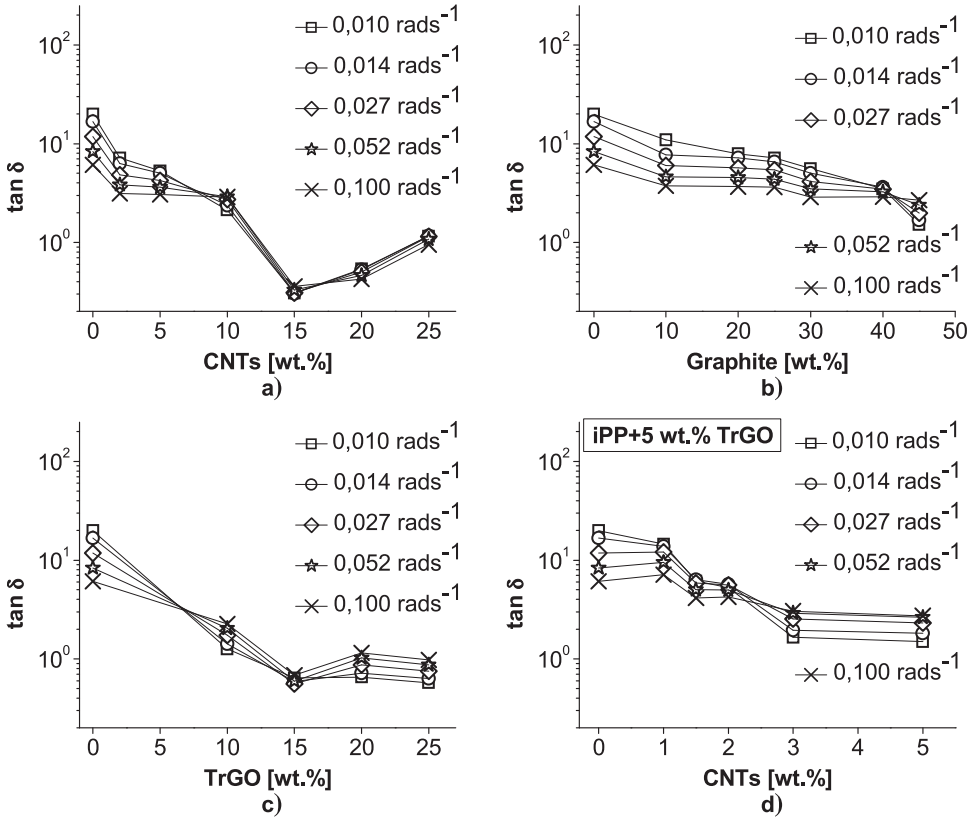

Figure 7. Loss tangent δ against filling degree φ of iPP composites with a) CNTs, b) graphite, c) TrGO, and d) 5 wt% of TrGO+CNTs for different angular frequencies ω, all measured at 190 °C. At the percolation threshold, δ becomes independent of ω.

filler percolation. In the case of polymer-CNTs composites, Pötschke et al.[48] reported that the immobility of the polymer chains determines the rheological percolation threshold. This immobility is due to combination of polymer and CNTs network formed by entanglements between polymer chains and CNTs, when two nanotubes are attached to each other within a distance less than the mean-square radius of gyration of the polymer chain.[46,48,49] The mean-square radius of gyration is given by[84,85]

$$\langle S^2 \rangle = a \cdot M^b \tag{10}$$

$$d = \sqrt{2 \cdot \langle S^2 \rangle} \tag{11}$$

where $\langle S^2 \rangle$ is the mean-square radius of gyration, M the molecular weight of the polymer, a and b are constant specifics for the iPP with values of 0.1156 and 1.0, respectively,[85] and d is the diameter of the polymer chain of 1000 monomers. In our case the iPP has polymer chains of ≈8570 monomers, and d is ≈ 9.12 nm. As a result, rheological percolation can be achieved when a nanotube network is partially but not completely constructed and the particle–particle distance is around 78 nm. In the case of electrical percolation, only the CNTs network contributes to conductivity.[49] The CNTs must directly be in contact with each other or locate within the distances smaller than the hopping distance of electrons,[11,65] which is in the range of a few nanometers. Consequently, it requires more conductive nanoparticles (CNTs) to approach the electrical percolation. However, in our iPP composites with carbon-based fillers, rheological percolations were greater than the electrical percolation, probably because of the inhomogeneous dispersion state, where both macroscopic aggregates and dispersed nanofillers contribute, similar to that reported in other studies.[36]

4. Conclusions

Our results showed that the kind of carbon-based filler (CNTs, graphite, and TrGO) had a significant impact on the mechanical behavior in the melt and solid state of iPP composites prepared by melt mixing. The iPP/TrGO composites presented the largest Young's modulus with values 15% higher (≈ 200 MPa) than iPP composites with graphite or CNTs. Moreover, by adding both the effect of the particle morphology and Young's modulus of the agglomerates within the Halpin–Tsai model the fit was improved, being possible to model the mechanical behavior of iPP composites in the solid state. The viscoelastic melt behavior of polymeric composites strongly depends on the filler used, increasing G' up to 5, 3, and 4 orders of magnitude at low frequencies when CNTs, graphite, and TrGO were used, respectively. While CNTs and graphite increase G' in the whole range of frequency, TrGO rendered unexpected lower values than iPP likely due to the iPP/TrGO interlayer slipperiness caused by the low surface friction of graphite. By adding a second carbon structure (CNTs) to iPP/TrGO composites, a relevant increase in the rheological behavior was further observed.

Acknowledgements: The authors gratefully acknowledge the Comisión Nacional de Investigación Científica y Tecnológica (CONICYT)-Chile for the doctoral fellowship and project FODECYT 1150130. The authors also expressed thanks to E.E. Mario Vergara, Chief of the Electrical Testing Unit (IDIEM)-Chile. The authors are also thankful to all persons of the Institut für Technische Chemie und Polymerchemie, Karlsruhe Institute of Technology (KIT), for the hospitality and collaboration provided during this investigation.

Received: October 19, 2015; Revised: November 24, 2015; Published online: February 2, 2016; DOI: 10.1002/mame.201500380

Keywords: carbon-based fillers; mechanical properties; nanocomposites; poly(propylene); rheology

[1] K. Chrissafis, D. Bikiaris, *Thermochim. Acta* **2011**, *523*, 1.
[2] Y. Jia, K. Peng, X. Gong, Z. Zhang, *Int. J. Plast.* **2011**, *27*, 1239.
[3] X. Chen, S. Wei, A. Yadav, R. Patil, J. Zhu, R. Ximenes, L. Sun, Z. Guo, *Macromol. Mater. Eng.* **2011**, *296*, 434.
[4] Q. He, T. Yuan, X. Zhang, Z. Luo, N. Haldolaarachchige, L. Sun, D. P. Young, S. Wei, Z. Guo, *Macromolecules* **2013**, *46*, 2357.
[5] Q. He, T. Yuan, J. Zhu, Z. Luo, N. Haldolaarachchige, L. Sun, A. Khasanov, Y. Li, D. P. Young, S. Wei, Z. Guo, *Polymer* **2012**, *53*, 3642.
[6] S. Wei, R. Patil, L. Sun, N. Haldolaarachchige, X. Chen, D. P. Young, Z. Guo, *Macromol. Mater. Eng.* **2011**, *296*, 850.
[7] E. Logakis, E. Pollatos, C. Pandis, V. Peoglos, I. Zuburtikudis, C. G. Delides, A. Vatalis, M. Gjoka, E. Syskakis, K. Viras, P. Pissis, *Compos. Sci. Technol.* **2010**, *70*, 328.
[8] C. Yang, H. Wei, L. Guan, J. Guo, Y. Wang, X. Yan, X. Zhang, S. Wei, Z. Guo, *J. Mater. Chem. A* **2015**, *3*, 14929.
[9] H. Wei, Y. Wang, J. Guo, N. Z. Shen, D. Jiang, X. Zhang, X. Yan, J. Zhu, Q. Wang, L. Shao, H. Lin, S. Wei, Z. Guo, *J. Mater. Chem. A* **2015**, *3*, 469.
[10] H. Palza, C. Garzón, O. Arias, *eXPRESS Polym. Lett.* **2012**, *6*, 639.
[11] C. Garzón, H. Palza, *Compos. Sci. Technol.* **2014**, *99*, 117.
[12] Y. P. Mamunya, V. V. Davydenko, P. Pissis, E. V. Lebedev, *Eur. Polym. J.* **2002**, *38*, 1887.
[13] T. Kashiwagi, E. Grulke, J. Hilding, R. Harris, W. Awad, J. Douglas, *Macromol. Rapid Commun.* **2002**, *23*, 761.
[14] T. Kashiwagi, E. Grulke, J. Hilding, K. Groth, R. Harris, K. Butler, J. Shields, S. Kharchenko, J. Douglas, *Polymer* **2004**, *45*, 4227.
[15] G. W. Lee, S. Jagannathan, H. G. Chae, M. L. Minus, S. Kumar, *Polymer* **2008**, *49*, 1831.
[16] Z. Spitalsky, D. Tasis, K. Papagelis, C. Galiotis, *Prog. Polym. Sci.* **2010**, *35*, 357.
[17] A. B. Sulong, M. I. Ramli, S. L. Hau, J. Sahari, N. Muhamad, H. Suherman, *Compos., Part B: Eng.* **2013**, *50*, 54.
[18] G. D. Liang, S. P. Bao, S. C. Tjong, *Mater. Sci. Eng., B* **2007**, *142*, 55.
[19] M. Wen, X. Sun, L. Su, J. Shen, J. Li, S. Guo, *Polymer* **2012**, *53*, 1602.

[20] S. P. Bao, G. D. Liang, S. C. Tjong, *IEEE Trans. Nanotechnol.* **2009**, *8*, 729.
[21] G. Zheming, L. Chunzhong, W. Gengchao, Z. Ling, C. Qilin, L. Xiaohui, *J. Ind. Eng. Chem.* **2010**, *16*, 10.
[22] Z. Y. Xiong, B. Y. Zhang, L. Wang, J. Yu, Z. X. Guo, *Carbon* **2014**, *70*, 233.
[23] T. D. Kelly, G. R. Matos, *U.S. Geol. Surv. Data Ser.* **2014**, *140*, 1.
[24] A. K. Geim, K. S. Novoselov, *Nat. Mater.* **2007**, *6*, 183.
[25] V. Singh, D. Joung, L. Zhai, S. Das, S. I. Khondaker, S. Seal, *Prog. Mater. Sci.* **2011**, *56*, 1178.
[26] H. Kim, A. Abdala, C. Macosko, *Macromolecules* **2010**, *43*, 6515.
[27] J. Zhu, M. Chen, Q. He, L. Shao, S. Wei, Z. Guo, *RSC Adv.* **2013**, *3*, 22790.
[28] W. S. Hummers, Jr., R. E. Offeman, *J. Am. Chem. Soc.* **1958**, *80*, 1339.
[29] P. Steurer, R. Wissert, R. Thomann, R. Mülhaupt, *Macromol. Rapid Commun.* **2009**, *30*, 316.
[30] J. R. Potts, D. R. Dreyer, C. W. Bielawski, R. S. Ruoff, *Polymer* **2011**, *52*, 5.
[31] M. J. McAllister, J.-L. Li, D. H. Adamson, H. C. Schniepp, A. A. Abdala, J. Liu, M. Herrera-Alonso, D. L. Milius, R. Car, R. K. Prud'homme, I. A. Aksay, *Chem. Mater.* **2007**, *19*, 4396.
[32] S. C. Tjong, *Express Polym. Lett.* **2012**, *6*, 437.
[33] L. Ren, X. Wang, S. Guo, T. Liu, *J. Nanopart. Res.* **2011**, *13*, 6389.
[34] T. Ramanathan, A. A. Abdala, S. Stankovich, D. A. Dikin, M. Herrera-Alonso, R. D. Piner, D. H. Adamson, H. C. Schniepp, X. Chen, R. S. Ruoff, S. T. Nguyen, I. A. Aksay, R. K. Prud'Homme, L. C. Brinson, *Nat. Nanotechnol.* **2008**, *3*, 327.
[35] Y. Guo, C. Bao, L. Song, B. Yuan, Y. Hu, *Ind. Eng. Chem. Res.* **2011**, *50*, 7772.
[36] K.-F. Ratzsch, V. Cecen, F. Tölle, K.-A. Wartig, R. Thomann, R. Mülhaupt, C. Friedrich, *Macromol. Mater. Eng.* **2014**, *299*, 1134.
[37] H. Kim, S. Kobayashi, M. A. AbdurRahim, M. J. Zhang, A. Khusainova, M. A. Hillmyer, A. A. Abdala, C. W. Macosko, *Polymer* **2011**, *52*, 1837.
[38] B. Dittrich, K.-A. Wartig, D. Hofmann, R. Mülhaupt, B. Schartel, *Polym. Degrad. Stab.* **2013**, *98*, 1495.
[39] P. Song, Z. Cao, Y. Cai, L. Zhao, Z. Fang, S. Fu, *Polymer* **2011**, *52*, 4001.
[40] M. A. Milani, R. Quijada, N. R. S. Basso, A. P. Graebin, G. B. Galland, *J. Polym. Sci., Part A: Polym. Chem.* **2012**, *50*, 3598.
[41] M. A. Milani, D. González, R. Quijada, N. R. S. Basso, M. L. Cerrada, D. S. Azambuja, G. B. Galland, *Compos. Sci. Technol.* **2013**, *84*, 1.
[42] H. Palza, B. Reznik, M. Wilhelm, O. Arias, A. Vargas, *Macromol. Mater. Eng.* **2012**, *297*, 474.
[43] D. Ahirwal, H. Palza, G. Schlatter, M. Wilhelm, *Korea-Australia Rheol. J.* **2014**, *26*, 319.
[44] Y. Li, J. Zhu, S. Wei, J. Ryu, L. Sun, Z. Guo, *Macromol. Chem. Phys.* **2011**, *212*, 1951.
[45] Y. Li, J. Zhu, S. Wei, J. Ryu, Q. Wang, L. Sun, Z. Guo, *Macromol. Chem. Phys.* **2011**, *212*, 2429.
[46] M. R. Nobile, *Wiley Encyclopedia of Composites*, Wiley, **2012**.
[47] O. Valentino, M. Sarno, N. G. Rainone, M. R. Nobile, P. Ciambelli, H. C. Neitzert, G. P. Simon, *Physica E* **2008**, *40*, 2440.
[48] P. Pötschke, M. Abdel-Goad, I. Alig, S. Dudkin, D. Lellinger, *Polymer* **2004**, *45*, 8863.
[49] Y. Pan, L. Li, *Polymer* **2013**, *54*, 1218.
[50] W. Thongruang, R. J. Spontak, C. M. Balik, *Polymer* **2002**, *43*, 3717.
[51] D. Bikiaris, *Materials* **2010**, *3*, 2884.
[52] K. Prashantha, *eXPRESS Polym. Lett.* **2008**, *2*, 735.
[53] B. H. Cipriano, A. K. Kota, A. L. Gershon, C. J. Laskowski, T. Kashiwagi, H. A. Bruck, S. R. Raghavan, *Polymer* **2008**, *49*, 4846.
[54] Y. Huang, S. Ahir, E. Terentjev, *Phys. Rev. B* **2006**, *73*, 125422.
[55] S. B. Kharchenko, J. F. Douglas, J. Obrzut, E. A. Grulke, K. B. Migler, *Nat. Mater.* **2004**, *3*, 564.
[56] K. Prashantha, J. Soulestin, M. F. Lacrampe, P. Krawczak, G. Dupin, M. Claes, *Compos. Sci. Technol.* **2009**, *69*, 1756.
[57] D. Xu, Z. Wang, *Polymer* **2008**, *49*, 330.
[58] X. Zhang, X. Yan, Q. He, H. Wei, J. Long, J. Guo, H. Gu, J. Yu, J. Liu, D. Ding, L. Sun, S. Wei, Z. Guo, *ACS Appl. Mater. Interfaces* **2015**, *7*, 6125.
[59] A. Kasgoz, D. Akin, A. Durmus, *Polym. Eng. Sci.* **2012**, DOI: 10.1002/pen.
[60] H. Kim, C. W. Macosko, *Macromolecules* **2008**, *41*, 3317.
[61] K. Wakabayashi, P. J. Brunner, J. Masuda, S. A. Hewlett, J. M. Torkelson, *Polymer* **2010**, *51*, 5525.
[62] K. Kalaitzidou, H. Fukushima, L. T. Drzal, *Carbon* **2007**, *45*, 1446.
[63] H. Kim, C. W. Macosko, *Polymer* **2009**, *50*, 3797.
[64] B. Yuan, C. Bao, L. Song, N. Hong, K. M. Liew, Y. Hu, *Chem. Eng. J.* **2014**, *237*, 411.
[65] H. Palza, C. Garzón, O. Arias, *eXPRESS Polym. Lett.* **2012**, *6*, 639.
[66] M. Rafiee, J. Rafiee, Z. Wang, H. Song, *ACS Nano* **2009**, *3*, 3885.
[67] M. Rafiee, J. Rafiee, I. Srivastava, Z. Wang, H. Song, Z.-Z. Yu, N. Koratkar, *Small* **2010**, *6*, 179.
[68] R. Sengupta, M. Bhattacharya, S. Bandyopadhyay, A. K. Bhowmick, *Prog. Polym. Sci.* **2011**, *36*, 638.
[69] K. Wakabayashi, C. Pierre, D. A. Dikin, R. S. Ruoff, T. Ramanathan, L. C. Brinson, J. M. Torkelson, *Macromolecules* **2008**, *41*, 1905.
[70] R. J. Young, I. A. Kinloch, L. Gong, K. S. Novoselov, *Compos. Sci. Technol.* **2012**, *72*, 1459.
[71] M. Mu, K. I. Winey, *J. Phys. Chem. C* **2007**, *111*, 17923.
[72] S.-Y. Fu, X.-Q. Feng, B. Lauke, Y.-W. Mai, *Compos., Part B: Eng.* **2008**, *39*, 933.
[73] J. C. Halpin, *Polym. Eng. Sci.* **1976**, *16*, 344.
[74] D. W. Schaefer, R. S. Justice, *Macromolecules* **2007**, *40*, 8501.
[75] M. Karevan, R. V. Pucha, A. Bhuiyan, K. Kalaitzidou, *Carbon Lett.* **2010**, *11*, 325.
[76] H. Palza, R. Vergara, P. Zapata, *Compos. Sci. Technol.* **2011**, *71*, 535.
[77] J. Vermant, S. Ceccia, M. K. Dolgovskij, P. L. Maffettone, C. W. Macosko, *J. Rheol.* **2007**, *51*, 429.
[78] C.-L. Huang, C. Wang, *Carbon* **2011**, *49*, 2334.
[79] G. Hu, C. Zhao, S. Zhang, M. Yang, Z. Wang, *Polymer* **2006**, *47*, 480.
[80] T. McNally, P. Pötschke, P. Halley, M. Murphy, D. Martin, S. E. J. Bell, G. P. Brennan, D. Bein, P. Lemoine, J. P. Quinn, *Polymer* **2005**, *46*, 8222.
[81] M. R. Nobile, in *Polym. Nanotub. Compos. Prep. Prop. Appl.* (Eds: T. McNally, P. Pötschke), Woodhead Publishing Limited, **2011**, pp. 428–481.
[82] M. Van Gurp, J. Palmen, *Rheol. Bull.* **1998**, *67*, 5.
[83] Y. Aoki, L. Li, M. Kakiuchi, *Macromolecules* **1998**, *31*, 8117.
[84] H. Palza, R. Vergara, P. Zapata, *Macromol. Mater. Eng.* **2010**, *295*, 899.
[85] Z. Zhou, D. Yan, *Macromol. Theory Simul.* **1997**, *6*, 597.
[86] Y. Qi, H. Guo, L. G. Hector, A. Timmons, *J. Electrochem. Soc.* **2010**, *157*, A558.